K. Zhang et al. *Swiss Journal of Geosciences* (2023) 116:3
https://doi.org/10.1186/s00015-023-00432-5

SGG SGS sc | nat
Swiss Journal of Geosciences

ORIGINAL PAPER Open Access

Sedimentary architecture of shallow-water fan-delta front in a lacustrine basin: Sangyuan section of Lower Cretaceous Xiguayuan Formation, Luanping Basin, northeast China

Ke Zhang[1,2,3*], Shenghe Wu[2*], Hehua Wang[1,3], Zhongrong Mi[1,3], Jianhua Qu[1,3*], Zhikun Wang[1,3] and Haonan Wang[2,4]

Abstract

The sedimentary architecture of fan deltas, which commonly constitute reservoirs, is a primary control on distribution and recovery efficiency of oil and gas. Deep-water fan deltas have been extensively discussed in the literature, whereas the sedimentary architecture of shallow-water fan-delta fronts, especially the characterization of mouth bar, quantification of architectural elements, and factors controlling the various architectural elements, remain poorly understood. Here, based on the integration of field survey and unmanned aerial vehicle (UAV) observation, the sedimentary architecture of Sangyuan section of the Lower Cretaceous Xiguayuan Formation in the Luanping Basin to is qualitatively and quantitatively characterized. Furthermore, factors controlling the architecture of the shallow-water fan-delta front are highlighted. Five facies associations, which differ in both lithofacies and dimensions, were interpreted in gravel-sand deposits of Sangyuan section, and indicate variations in flow conditions during deposition. The width/thickness ratio of facies associations generally increases rapidly as the flow energy and flow concentration decreases from debris flow to traction currents during the evolution of shallow-water fan delta. Both distributary channels and mouth bars dominate facies associations in the shallow-water fan-delta front, accounting for 53.42% and 36.88% of gravel-sand deposits respectively in Sangyuan section. Mouth bar consists of gravel accretions and sand accretions. Grain size of sediments influences the relative strength of the inertial force and bed friction, which determine the effluent behavior in a river-mouth system and the vertical grain-size trend of mouth bar accretions. Gravel accretions are characterized by normal grading, and these are interpreted as the products of inertia-dominated effluent. Sand accretions exhibit coarsening-upward trends in the river-mouth systems where friction-dominated outflow occurred. The overall vertical grain-size trend of mouth bar depends on the stacking pattern of accretions rather than the grading of one accretion.

Keywords Shallow-water fan delta, Distributary channel, Mouth bar, Dimension, Accretion, Effluent behavior

Editorial handling: Wilfried Winkler

*Correspondence:
Ke Zhang
zhangke@zhenhuaoil.com
Shenghe Wu
reser@cup.edu.cn
Jianhua Qu
qujianhua@zhenhuaoil.com

[1]China Zhenhua Oil Co. Ltd, Beijing, China.
[2]China College of Geosciences, State Key Laboratory of Petroleum Resources and Prospecting, China University of Petroleum, Beijing, China.
[3]Chengdu Northern Petroleum Exploration and Development Technology Co. Ltd, Chengdu, Sichuan, China.
[4]Chengdu Exploration and Development Research Institute of PetroChina Daqing Oilfield Co. Ltd, Chengdu, Sichuan, China.

Springer Open

© The Author(s) 2023. **Open Access** This article is licensed under a Creative Commons Attribution 4.0 International License, which permits use, sharing, adaptation, distribution and reproduction in any medium or format, as long as you give appropriate credit to the original author(s) and the source, provide a link to the Creative Commons licence, and indicate if changes were made. The images or other third party material in this article are included in the article's Creative Commons licence, unless indicated otherwise in a credit line to the material. If material is not included in the article's Creative Commons licence and your intended use is not permitted by statutory regulation or exceeds the permitted use, you will need to obtain permission directly from the copyright holder. To view a copy of this licence, visit http://creativecommons.org/licenses/by/4.0/.

1 Introduction

Fan delta is defined as an alluvial fan prograding directly into a standing body of water from an adjacent highland (Holmes, 1965; McPherson et al., 1987; Nemec & Steel, 1988). As the crucial deposits in the margin of basin, fan deltas are commonly potential reservoirs for hydrocarbon and coals (Ziegler, 2001; Poppelreiter and Aigner, 2003; Liu et al., 2019), and thus, these deposits are of significant interest to researchers.

According to the bathymetry data (ratio of channel to basin depth), fan deltas can be categorized into shallow-water and deep-water types (Ethridge & Wescott, 1984; Postma, 1990). Shallow-water fan deltas are characterized by gently inclined delta fronts and are dominated by topsets, whereas deep-water fan deltas (also called Gilbert-type fan delta) involve steeply inclined delta front and are dominated by foresets (Edmonds et al., 2011). Sedimentary characteristics (Postma & Roep, 1985; Rohais et al., 2008; Longhitano, 2008; Backert et al., 2010), depositional process (Falk & Dorsey, 1998; McConnico & Bassett, 2007), and factors controlling the Gilbert-type fan delta deposits (Colella, 1988; Zhong et al., 2018; Barrett et al., 2019) have been extensively investigated. Based on field observations, flume experiments and numerical simulations, examples of shallow-water fan deltas have also been reported. However, these studies reveal that the sedimentary architecture of shallow-water fan-delta front differ significantly, especially in the extent of development and vertical gradation of mouth bar.

The extent of development of mouth bars remains a topic of debate among researchers. According to the data from outcrops and reservoir description, distributary channels are dominant in fan-delta fronts, while mouth bars are undeveloped or minor in scale (Jia et al., 2000; Dou et al., 2020; Wu et al., 2020). Jia et al. (2000) characterized facies associations in the Xiguayuan Formation in the Luanping Basin and assigned 64.59% of facies to distributary channels, and only 1.4% to mouth bars in the fan-delta front. Conversely, according to other studies, both distributary channels and mouth bars are dominate facies associations in fan-delta front (Billi et al., 1991; Van Dijk et al., 2009; Wang et al., 2015; Zhang et al., 2021, 2022a, 2022b). Billi et al. (1991) indicated that the shallow water, small size, and low energy of the lake favored the formation of mouth bars in the fan-delta front. Physical experiments have been used to reconstruct the formation of mouth bar in shallow-water fan delta. Major isolated mouth bars develop near the shoreline if the channel is narrow and deep, whereas multiple arrays of mouth bars with small scale are formed at the river mouth if the channel is wide and shallow (Van Dijk et al., 2009; Wang et al., 2015; Zhang et al., 2021). The development of mouth bars and distributary channels in shallow-water fan deltas have also been investigated via stochastic simulations using the parallel multi-stage GAN (Zhang et al., 2022b). According to a 3D model, proportions of mouth bars and distributary channels are 48.6% and 24.7%, respectively.

The vertical grain-size trends of mouth bar in the fan-delta front are complex. Field observations and reservoir characterization studies reveal that mouth bars comprise coarsening-upward sand sequences (Billi et al., 1991; Jia et al., 2018). However, some studies based on outcrops describe fining-upward trend of mouth bars in shallow-water fan deltaic successions (Benvenuti, 2003; Fabbricatore et al., 2014). Besides, in flume experiment of shallow-water fan delta, the fining-upward mouth bar developed (Wang et al., 2015). Therefore, the sedimentary architecture of shallow-water fan deltas, especially the mouth-bar characterization, requires further investigation. In addition, the following aspects of the sedimentary architecture still remain poorly understand: (i) quantitative descriptions because previous studies mainly qualitative and (ii) controlling factors.

Here, field surveys and unmanned aerial vehicle observations were utilized to study the Sangyuan section of the Lower Cretaceous Xiguayuan Formation in the Luanping Basin. The objectives of the present study were as follows: (i) to qualitatively and quantitatively characterize the sedimentary architecture of a shallow-water fan-delta front and (ii) to elucidate factors controlling sedimentary architecture.

2 Geological setting

The Luanping Basin is an extensional basin in the north of the Yanshan Fold-thrust Belt in northeast China (Graham et al., 2001; Davis et al., 2001; Ren et al., 2002; Cope and Grahanm, 2007; Wei et al., 2012). This simple half-graben, which is bounded by normal faults on the northwest and west (Wu et al., 2000; Cope et al., 2010; Yan et al., 2020), developed during Late Jurassic–Early Cretaceous time, period. The basin displays a NE-SW orientation, and it is approximately 40 km long and 20 km wide, thereby covering an area of almost 800 km^2 (Fig. 1). The basement comprises Archean metamorphic and Proterozoic intrusive rocks, overlain by Middle Jurassic, Upper Jurassic and Lower Cretaceous strata. Lower Cretaceous strata host the Dadianzi and Xiguanyuan formations (Li et al., 2004; Tian et al., 2004). The initial-rift, rift-climax and rift-recession succession have been documented in Xiguayuan Formation, and a complete alluvial fan–lacustrine sequence has been reported, consisting of alluvial fan, fan-delta and lacustrine facies associations (Cope et al., 2010; Dou et al., 2020; Jia et al., 2020).

The Sangyuan section lies in western part of Luanping Basin, approximately 20 km from the Luanping District.

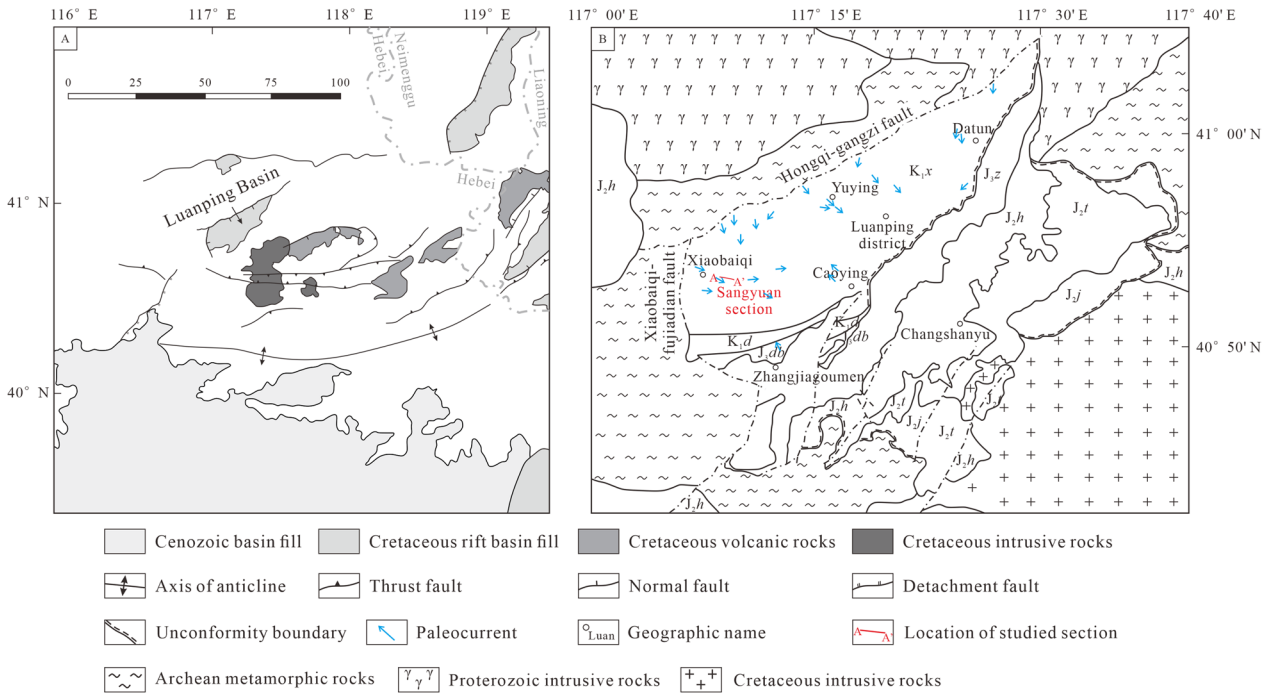

Fig. 1 Maps showing the **A** location of the Luanping Basin in the north of a fold-thrust belt, and **B** detailed structure, exposed stratigraphic formation, paleocurrent direction, and locations of the section studied. J_2j-Jiulongshan Formation, J_2t-Tiaojishan Formation, J_2h-Houcheng Formation, J_3z-Zhangjiakou Formation, J_3db-Dabeigou Formation, K_3d-Dadianzi Formation, K_3x-Xiguayuan Formation

Paleocurrent indicators in the section suggest a NW direction. According to previous studies, shallow-water fan delta deposits in the Sangyuan section are characterized by coarse-grained sediments with various sedimentary structure, which indicate the coexistence of traction and gravity flows, and are dominated by topset beds. The widespread distribution of symmetrical ripples and mud cracks in Sangyuan section indicate deposition in shallow-water to subaerial environments (Zhang et al., 2022a). From the southeast to the northwest (lower part to upper part of Sangyuan section), the thickness of gravel-sand deposits gradually decreases and then increases along with the fluctuation of lake level. Luo et al. (2007) identified six 5th base level cycles (namely, SQ1–SQ6) in the Sangyuan section. SQ1–SQ3 represent fining- and thinning-upward sequences, whereas SQ4–SQ6 exhibit coarsening- and thickening-upward trends (Fig. 2).

3 Data and methodology

In this study, field surveys and unmanned aerial vehicle (UAV) observations were integrated. Field surveys were used to closely examine lithologies, sedimentary structures and vertical grain-size trends of gravel-sand deposits. Based on field surveys, more than 400 high-definition photographs of the section were taken and 17 columns with a cumulative length of approximately 420 m describing the sedimentary architecture were drawn. Moreover, 18 samples were collected to examine grain-size variations in mouth bar deposits, whereas 24 samples (S1–S24 in Fig. 2) were taken to investigate fluctuations of the lake level using geochemical analyses data. All analyses were conducted in the State Key Laboratory of Petroleum Resources and Prospecting, China University of Petroleum (Beijing).

The UAV observation is a research method that is used to collect data from different locations, and these data can be employed to establish a three-dimensional (3D) model of a studied area. This method enables the collection of data from high and steep mountain areas, as well as other areas that are inaccessible through field surveys. The 3D digital model that is established from these data facilitates quantitative analysis that is void of manual measurement errors and subjective direct observations (Blistan et al., 2016; Yin et al., 2018). In the present study, a UAV equipped with an oblique camera that contains five lenses was utilized, and the observation altitude was 300 m. More than 5500 photographs involving coordinates were taken during observations, and the resolution of the established digital model is 0.2 m. This model was used to investigate the macroscopic distribution and quantitative scales of architectural elements.

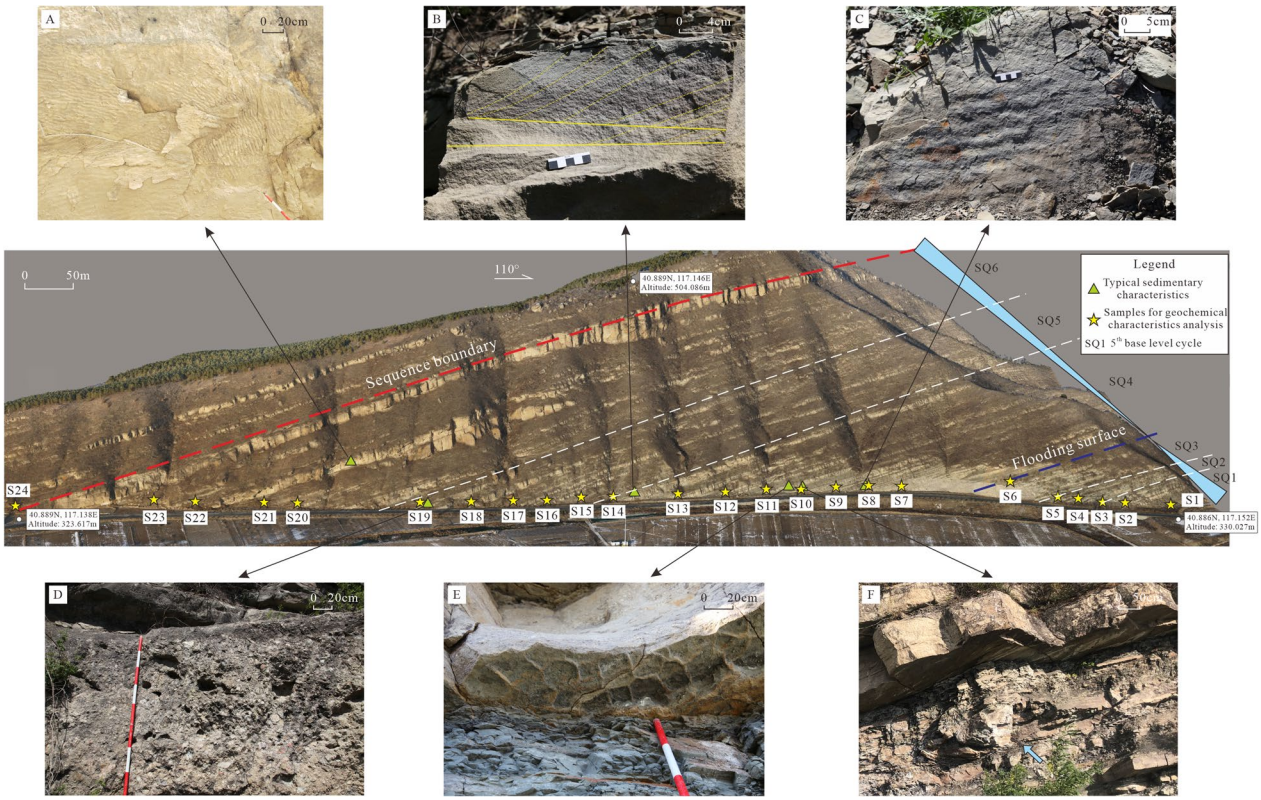

Fig. 2 3D digital model of the Sangyuan section that was established based on UAV observations data. From the bottom to top, the thickness of gravel-sand deposits gradually decreases, and then it increases according to fluctuations of the lake level. **A** symmetrical ripples that indicate a shallow-water environment above the wave base; **B** cross-laminated sandstones reflecting actions of traction currents; **C** symmetrical ripples; **D** coarse-grained sediments; **E** mud cracks that are indicative of a subaerial environment; **F** slump structures associated with gravity flow deposits

4 Sedimentary characteristics and analysis

4.1 Lithology

According to grain sizes, lithofacies in the shallow-water fan delta include conglomerate, sandstone and mud–siltstone. Based on sedimentary structures, twelve subtypes including C1–C6, S1–S5, and M1were identified (Fig. 3).

4.1.1 Conglomerate lithofacies

In this lithofacies, grains with diameters that are > 2 mm exceed 30%, and the main subtypes include pebble conglomerate, granule conglomerate and graded conglomerates.

A. Pebble conglomerate

In this subtype of the conglomerate lithofacies, content of grains with diameters that are > 10 mm is higher than 50%. Based on sedimentary structures, it can be divided into massive pebble conglomerate (C1) and imbricated pebble conglomerates (C2).

The massive pebble conglomerate is clast- or matrix-supported, and it is characterized by relatively poor grain sorting. Clasts are randomly arranged, and nearly upright gravels and muddy rip-up clast occur occasionally (Fig. 3A). Conversely, the imbricated pebbly conglomerate is clast-supported and extremely poorly sorted. It contains gravels that are up to 10 mm long, and these display a consistent NNS orientation (Fig. 3B).

B. Granule conglomerate

Grains with diameter varying between 2 and 10 mm are > 50% in this conglomerate subtype. Sedimentary structures reveal that this subtype involves massive granule conglomerate (C3), cross-laminated granule conglomerate (C4), and imbricated granule conglomerate (C5).

The massive granule conglomerate is clast-supported and poorly sorted. It contains gravels that exhibit random orientations and muddy rip-up clasts in its lower portion (Fig. 3C). The cross-laminated granule conglomerate is also clast-supported, but it is characterized by

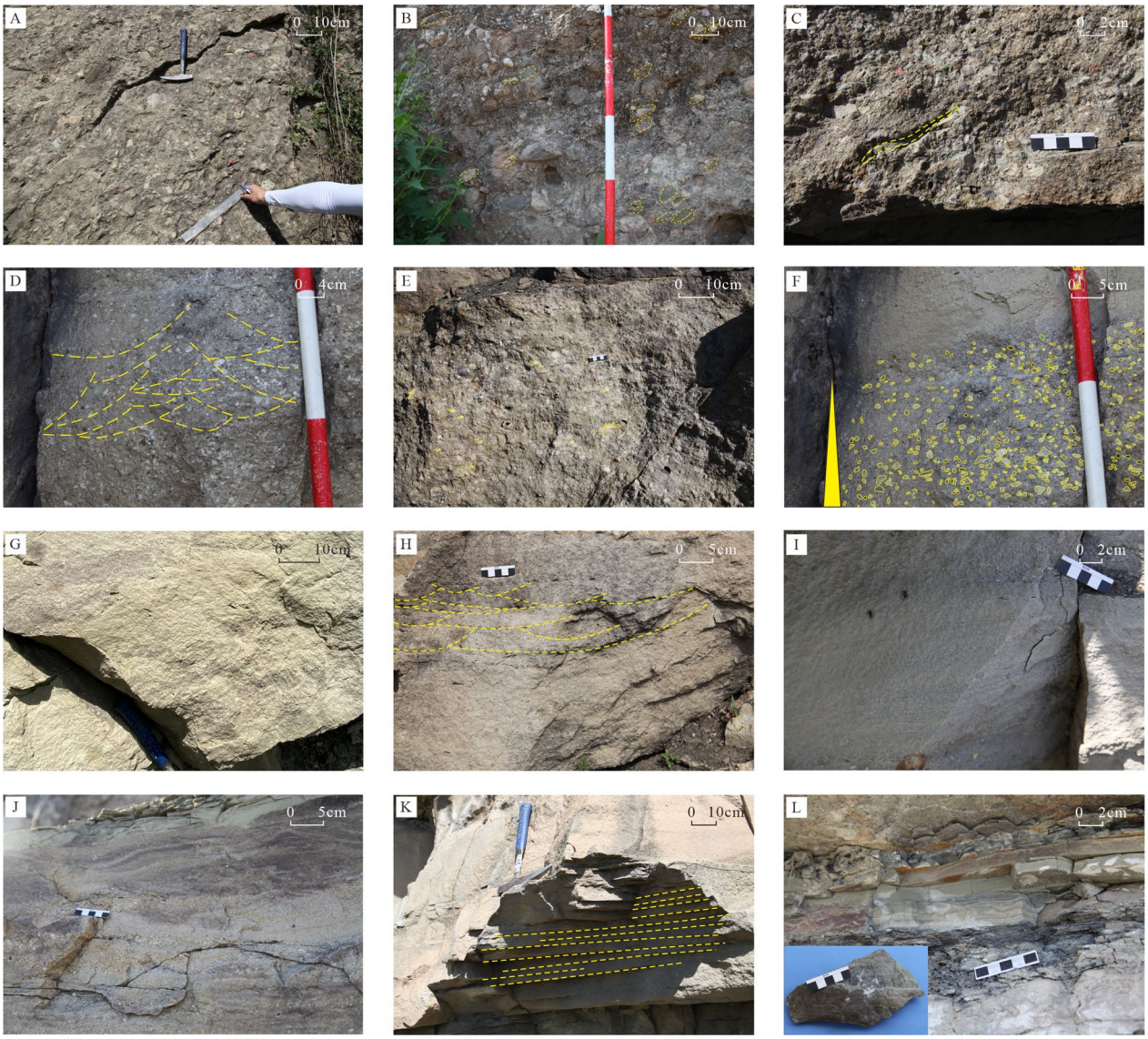

Fig. 3 Lithofacies in Sangyuan section. **A** massive pebble conglomerate (C1); **B** imbricated pebble conglomerate (C2); **C** massive granule conglomerate (C3); **D** cross-laminated granule conglomerate (C4); **E** imbricated granule conglomerate (C5); **F** grading conglomerate (C6); **G** massive coarse sandstone (S1); **H** cross-laminated coarse sandstone (S2); **I** parallel-laminated coarse sandstone (S3); **J** cross-laminated fine to medium sandstone (S4); **K** parallel-laminated fine to medium sandstone (S5); **L** mud–siltstone (M1)

moderately sorted grains. Steep inclinations (up to 60°) and thick (thicknesses of 5–15 cm) cross-laminations are typical features of this conglomerate type. Randomly oriented gravels and some that are arranged along bedding planes are also present (Fig. 3D). In the imbricated granule conglomerate, gravels commonly display an orientation that is indicative of the paleocurrent direction (Fig. 3E).

C. Graded conglomerate

In this conglomerate type, grains with diameters that are > 10 mm and between 2 and 10 mm make up < 50%. The relatively wide grain size distribution accounts for its poor sorting. This graded conglomerate (C6) exhibits either normal or inverse grading (Fig. 3F).

4.1.2 Sandstone lithofacies

Based on grain sizes, the sandstone lithofacies is divided into coarse sandstone and fine–medium sandstone.

A. Coarse sandstone

In this subtype, coarse sand grains are > 50%, and it can be subdivided into massive coarse sandstone (S1), cross-laminated coarse sandstone (S2), and parallel-laminated coarse sandstone (S3).

The massive and cross-laminated coarse sandstones are moderately sorted, and these contain < 5% of conglomerate grains with relatively small diameters (Fig. 3G and H). Conglomerates in cross-laminated coarse sandstone are arranged along bedding planes. Conversely, parallel-laminated coarse sandstones are well sorted (Fig. 3I). Compared with the cross-laminated granular conglomerate, inclinations of bedding planes are gentle (between 2 and 20°) and the scale of cross-lamination is lower (laminas are < 10 cm thick) (Fig. 3H).

B. Fine–medium sandstone

The fine–medium sandstone lithofacies contains mainly fine and medium sand grains. Sedimentary structures enabled this sandstone type to be classified as cross-laminated (S4) and parallel-laminated (S5), and both subtypes are well sorted (Fig. 3J and K).

Cross-laminated fine–medium sandstone displays trough and wedge-shaped cross bedding, as well as ripple laminations. The fine sand content gradually increases while the scale of cross-lamination decreases from the trough cross bedding-dominated (medium sand-dominated, and laminas are < 5 cm) to the ripple lamination-dominated (fine sand-dominated and laminae are < 2 cm) fine–medium sandstones (Fig. 3J).

4.1.3 Mud–siltstone lithofacies

This lithofacies (M1), which contains abundant clay and silt, varies from light green to gray-green and dark gray. In deposits with high silt contents, ripple laminations developed locally, whereas occasional mud cracks in light gray mudstones reflect deposition in a subaerial environment (Fig. 3L).

4.2 Characteristics of the sedimentary architecture and analysis

Even though the studied section was occasionally exposed to the subaerial environment, it was primarily deposited in a shallow-water environment, and thus, records preserved are mostly those of shallow-water fan-delta front deposits. Three facies associations emerged from the gravel-sand deposits, and these included distributary channel, lobe and sheet sand deposits. Deposits containing mud–siltstone are not the focus of this study.

4.2.1 Facies association A–Distributary channel

Description

Facies association A consists of conglomerate and coarse sandstone, and this is characterized by normal grading and concave-up beds with erosional bases. Distributary channel deposits vary from 1 to 28 m in thickness between 6 and 160 m in width. Scale, lithofacies associations, and nearby bedding plane structures partition distributary channel deposits into types A and B. Type A channel deposits (FAA) are characterized by coarse-grained sediments and thick beds, which are overlain by light green and greenish gray mud–siltstones. The mud cracks can be seen nearby. The lower portion of the FAA, which involves the C1 and C2 lithofacies, is > 5 m thick, and this is overlain by the C3 and C5 lithofacies (Fig. 4). Type B channel deposits (FAB) vary in thickness from a few decimeters to 4 m, and it contains a higher proportion of fine sediments than the FAA. The lower portion generally comprises the C3, C4, and C6 lithofacies, and these are overlain by the S1, S2 and S3 (Fig. 5). Associated greenish to dark gray mud–siltstones and ripples occurs around occasionally.

Interpretation

The FAA is in the SQ6 and it is attributed to deposition in subaerial distributary channels. The associated mud cracks and light color of mud–siltstones likely reflect the subaerial environment. The presence of randomly oriented gravels, poor sorting, and lack of grading in lithofacies C1 and C3 are attributed to highly concentrated debris flows that were devoid of internal laminar shearing (Gloppen & Steel, 1981; Shanmugam, 2000; Gani, 2004). The C2 and C5 lithofacies are extremely poorly sorted and the common occurrence of large oriented clasts suggests deposition from weak-cohesive debris flows. Large gravels can be moved and turned by currents because of weak cohesion, and this probably explains the imbrication in conglomerates (Hampton, 1975; Lowe et al., 1982; Zavala & Pan, 2018).

Sediments in the FAB are attributed to deposition in subaqueous distributary channels. Symmetrical ripples and relatively dark color of the associated mud–siltstones suggest deposition in a shallow-water environment. As shown in Fig. 5, characteristics of subaqueous

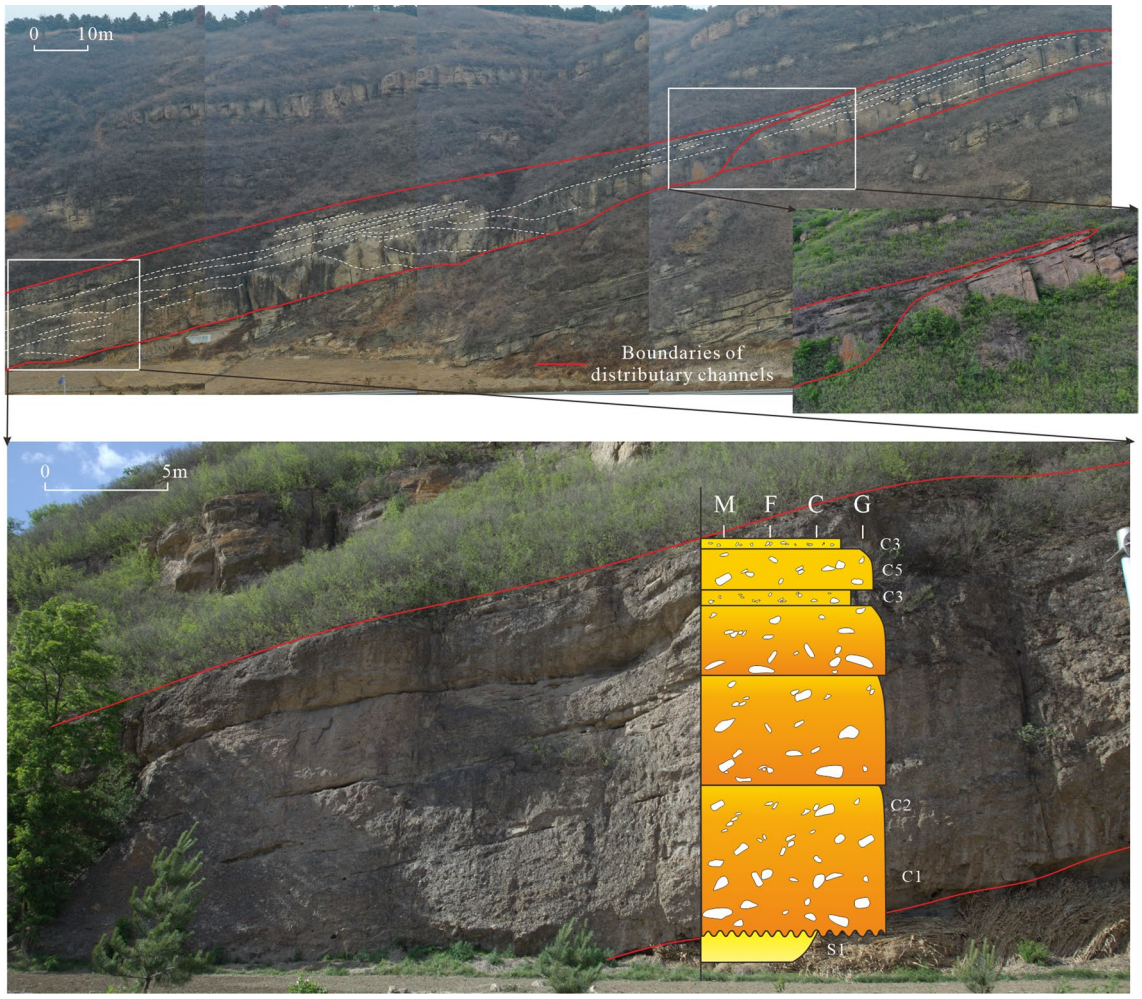

Fig. 4 Sedimentary architecture of type A channel deposits. Lithofacies C1 and C2 that are in the bottom portion exceed 5 m in thickness, and these are overlain by the C3 and C5 lithofacies

distributary channels are complex because of the presence of diverse lithofacies associations. Lithofacies variations probably represent the change of flow conditions. Inverse graded and overlying normal graded units can be interpreted as products of a hyperpycnal flow, which reflects expanding-to-waning flash floods (Zavala et al., 2006; Yan et al., 2020) (Fig. 5b1). The C3 lithofacies is attributed to a non-tractional deposition because of its poor sorting, occurrence of randomly oriented gravels and muddy rip-up clasts. Conversely, the S2 and S3 lithofacies are assigned to fully tractional deposition, and these display the upper flow-regime plane-bed configuration as well as dunes and current ripples (Benvenuti et al., 2003). Thus, lithofacies associations involving the C3 overlain by the S2 are connected to the genesis of debris flows to traction currents (Fig. 5a2). During evolution of the fan delta (decreasing scale of distributary channels), products of debris flow decreased in thickness, whereas those of traction currents, such as the cross-laminated conglomerate and sandstone, are more likely to be recorded (Fig. 5a1).

4.2.2 Facies association B–Lobe

Description

Facies association B typically contains conglomerates and sandstones, and these strata exhibit convex-upward top surfaces. Individual units range from 1 to 15 m in thickness and generally extend laterally for >60 m. Based on differences in lithofacies associations and vertical grain-size trends, this lithofacies can be associated with the following lobe types: gravel lobes (FBA) and gravel-sand lobes (FBB).

The FBA is characterized by coarse-grained sediments (dominated by the C1 and C3 lithofacies) and the lack of a grain-size trend. It ranges from 8 to 15 m in thickness

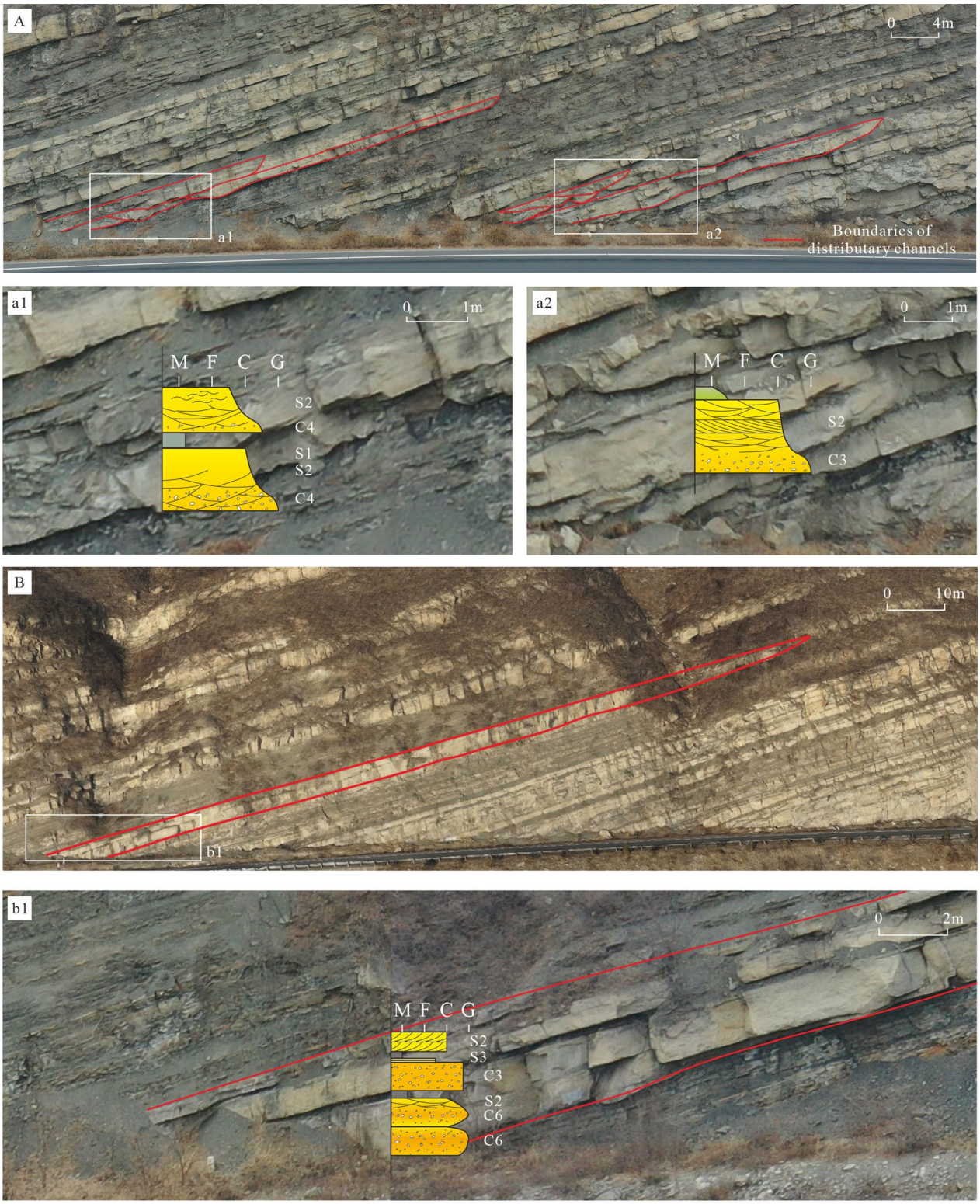

Fig. 5 Sedimentary architecture of type B channel deposits. Lithofacies associations in type B channel deposits are complex, but in general, these involve the C3, C4, and C6 in the bottom, which are overlain by the S1, S2 and S3

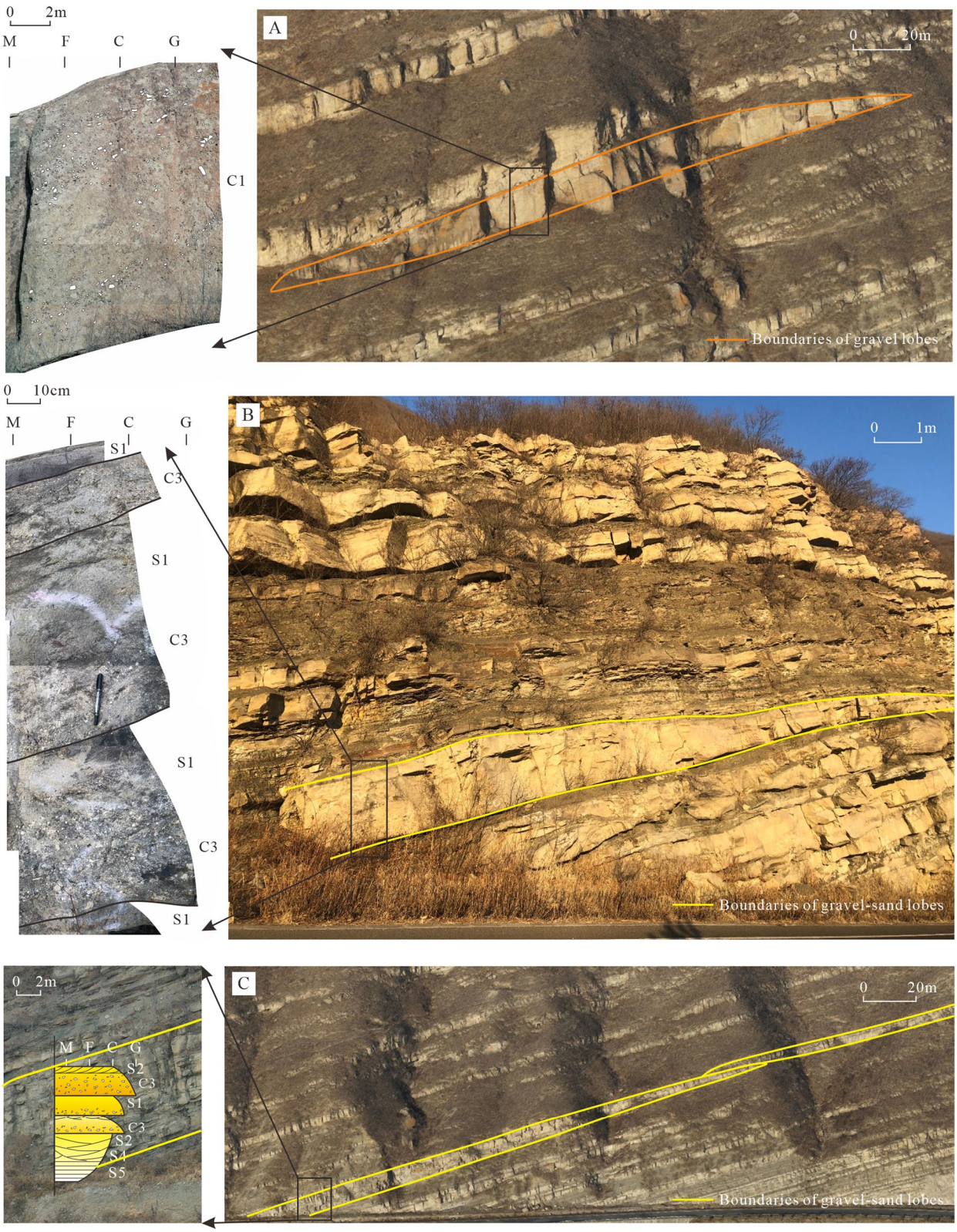

Fig. 6 Sedimentary architecture of lobes. **A** Gravel lobes that are characterized by coarse-grained sediments and no grain-size trend; **B** gravel accretions comprising primarily of the C3 lithofacies overlain by S1, five normally-graded accretions are recognized in this gravel-sand lobe; **C** sand and gravel accretions, sand accretions generally contain cross- and parallel-laminated sandstones that are characterized by coarsening-upward trends

and 60–150 m in lateral extent (Fig. 6A). Sand and gravel accretions are recognized in the FBB. Gravel accretions (the thickness of the conglomerate lithofacies accounts for > 30%) primarily contain the C3 lithofacies overlain by the S1 (Fig. 6B). Sand accretions are generally cross- and parallel-laminated sandstones that comprise the S2, S3, S4, and S5 lithofacies (Fig. 6C). These accretions and the FBB display either coarsening- or fining-upward trends.

Interpretation

The FBA is common in the SQ6. Its spatial distribution and low width/thickness ratios of 8–10 imply that it originated from highly concentrated flows at the lake margin. Its massive coarse-grained sediments, occurrence of upright gravels, and lack of a grain-size trend suggest its deposition involved a freezing process by debris flows (Kim, 1995; Sohn et al., 1999). This caused lobes to extend forward instead of laterally (Van Dijk et al., 2009; Zhang et al., 2021), and thus, the FBA is assigned to tongue-shaped debris deposits. It was likely derived from debris deposits in alluvial fans that were dipping into the lake (Blair & McPherson, 1998; Wu et al., 2016).

The FBB also displays a convex-upward top surface, and its non-erosive bed contact and upward-fining or upward-coarsening sequences suggest that it is a mouth bar deposit. Accretions in the FBB are considered records of the progradation of mouth bar bodies. Grain size variations in accretions probably reflect a continuous river supply that was characterized by variable flow discharge and energy. Gravel accretions represent mouth bar deposits from fluvial processes at the river mouth of subaerial distributary channels or a main/proximal subaqueous distributary channel (Dunne & Hempton, 1984; Rasmussen, 2000). The massive appearance and normal grading of gravel accretions imply that these originated from debris flows (Shultz, 1984; Rasmussen, 2000). In fact, the massive gravelly bed (C3 lithofacies) was deposited abruptly as an inertial carpet, whereas turbulent currents continued to deposit sand (S1 lithofacies) (Benvenuti, 2003; Fabbricatore et al., 2014). Conversely, sand accretions were probably deposited at outlets of secondary/distal subaqueous distributary channels (Rasmussen, 2000; Fabbricatore et al., 2014). Sand lithofacies that are characterized by slightly inclined cross- and parallel-lamination are attributed to traction currents in the river mouth system (Turner & Tester, 2006; Winsemann et al., 2009).

4.2.3 Facies association C–Sheet sand

Description

Facies association C generally involves the S4 (dominated by ripple lamination) and S5 lithofacies, as well as occasional ripple-laminated siltstone, and it displays a sheet-like geometry. Its thickness ranges from 0.3 to 0.8 m and extend laterally for hundreds of meters. The lateral boundaries of sheet sand deposits are poorly exposed because of vegetation cover, and this explains the general lack of exact width values (Fig. 7). This facies

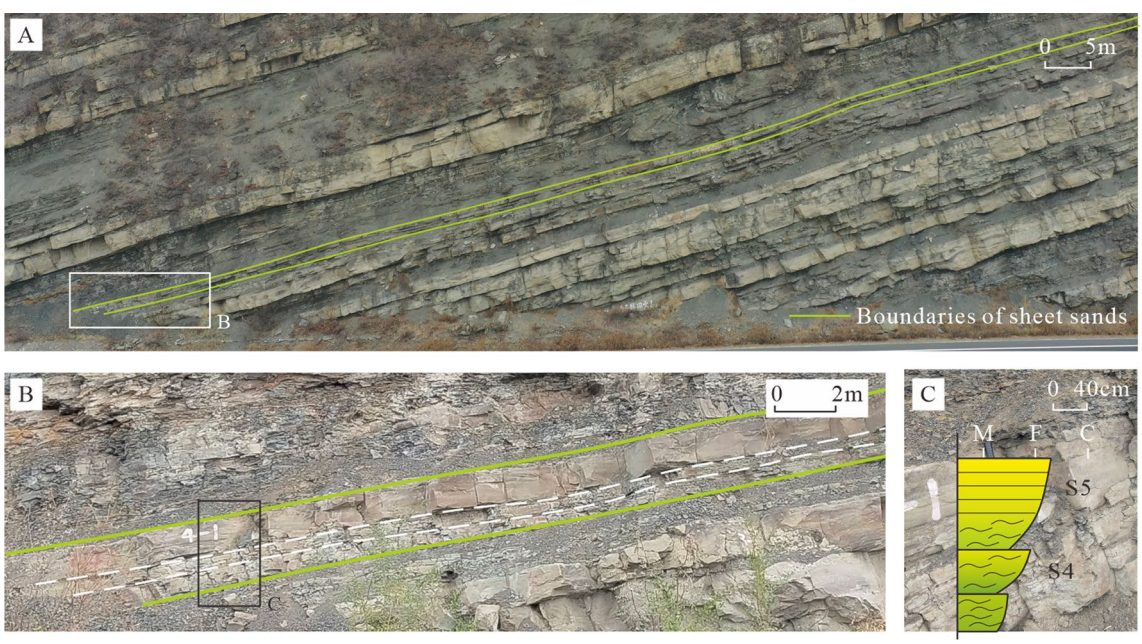

Fig. 7 Sedimentary architecture of sheet sand, which commonly contain the S4 (dominated by ripple laminations) and S5 lithofacies

association occurs near symmetrical ripples and dark gray mud–siltstones.

Interpretation

These laterally extensive sheets are interpreted to represent sheet sand deposits from traction currents via reworking of sands that were previously deposited in the shallow-water fan-delta front (Orton & Reading, 1993; Longhitano, 2008). Ripple cross-laminated sandstones probably represent the phase of deposition involving waves of variable energy. Dark mud–siltstones and fine sandstones indicate low energy conditions also occurred during deposition.

4.3 Dimensions of architectural elements

Based on the characteristics of architectural elements, especially the lithofacies associations and geometry, their spatial distribution in the shallow-water fan-delta front is elucidated (Fig. 8). Dimensions of architectural elements, including distributary channels, tongue-shaped debris deposits, mouth bars, and sheet sands, were measured using the 3D digital model of the studied section. According to the results, the proportion of gravel-sand deposits in the Sangyuan section is 31.67%. Distributary channel and mouth bar deposits dominate facies associations in the shallow-water fan-delta front as reported by Billi et al. (1991), and these account for 53.42% and 36.88%, respectively. Tongue-shaped debris deposits and sheet sands correspondingly represent 8.39% and 1.31% of the gravel-sand deposits.

The relationship between the thickness and width of architectural elements (after corrections associated with directions) are shown in Fig. 9. Sheet sands exhibited the highest width/thickness ratios (higher than 121) as it ranges from 0.3 to 0.8 m in thickness and often show a considerably lateral extent (wider than 100 m). Conversely, tongue-shaped debris deposits produced a

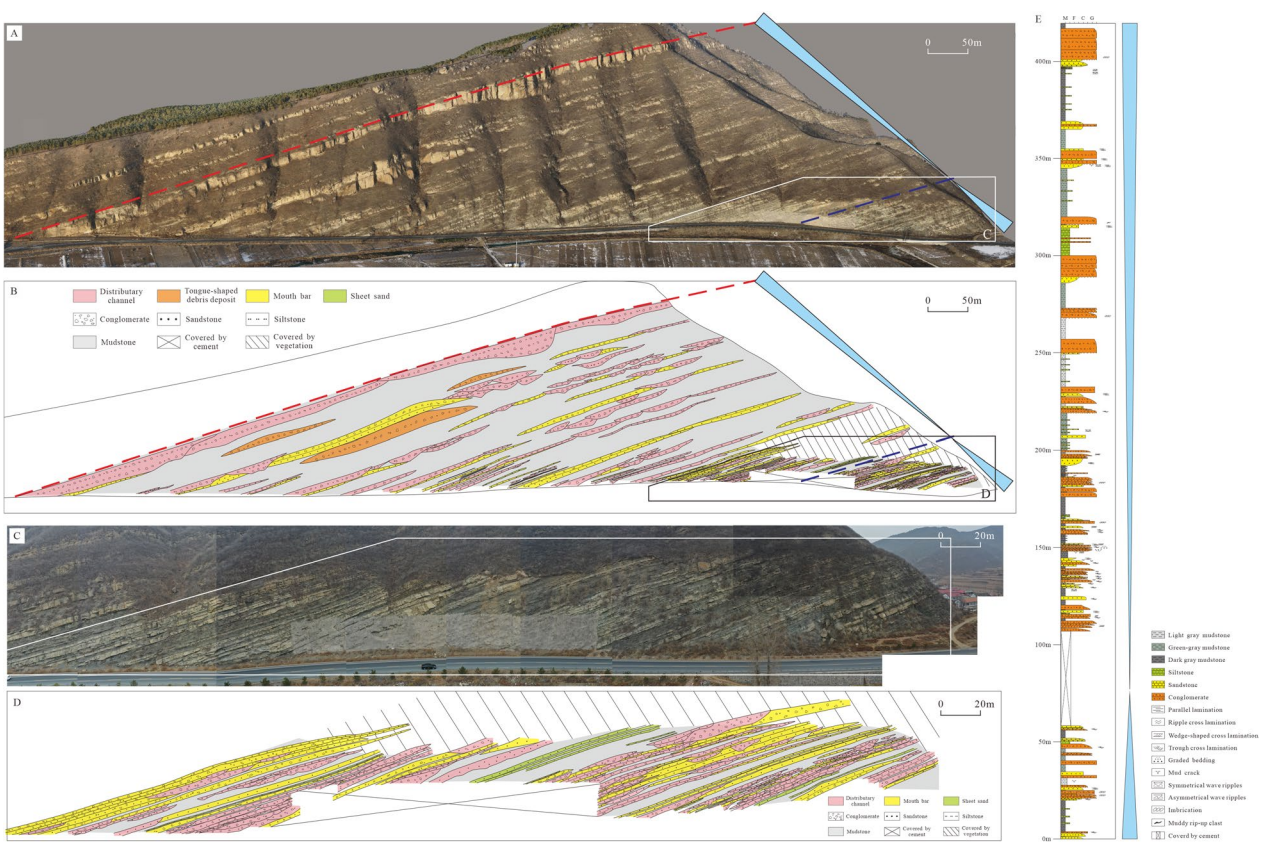

Fig. 8 Distribution of architectural elements in the shallow-water fan delta front in the Sangyuan section. **A** The 3D digital model of studied section. **B** The interpretation of the sedimentary architecture. **C** and **D** Magnification of images shown in (**A**) and (**B**). **E** Column of Sangyuan section. The proportion of gravel-sand deposits in the Sangyuan section is 31.67%. Distributary channels and mouth bars dominate facies associations in the shallow-water fan delta front

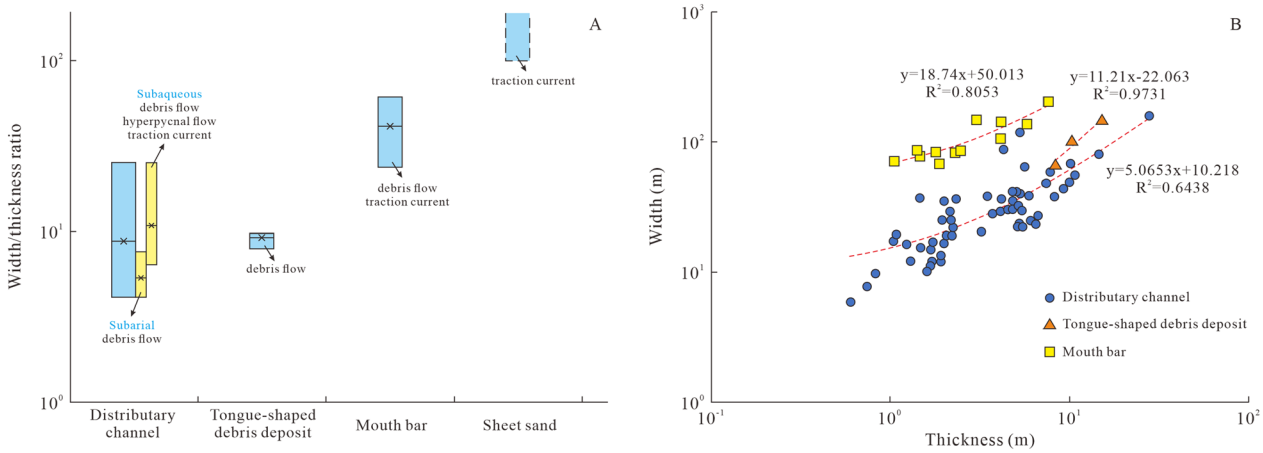

Fig. 9 Plots showing dimensions of architectural elements measured via the 3D digital model. **A** The width/thickness ratio of architectural elements increased rapidly as the flow energy and concentration changed from debris flow to traction currents during the shallow-water fan delta evolution. **B** The width is positively correlated with thickness for each architectural element, however, the correlation coefficients differ

narrow range of width/thickness ratios (8–10), and the average was 9.1. Relatedly, mouth bars showed width/thickness ratios that range from 23 to 67, and the average was 41.3. Subaerial and subaqueous distributary channels showed width/thickness ratios of 4–7 (averaging 5.3) for the former and 6–25 (averaging 10.7) for the latter. Overall, width/thickness ratios of architectural elements increased rapidly as the flow energy and concentration changed from those of debris flows to traction currents during evolution of the shallow-water fan delta (Fig. 9A). Variations in flow conditions during deposition in subaqueous distributary channels and mouth bars likely account for the extensive differences in width/thickness ratios.

Regarding architectural elements, the width and thickness data for each exhibit positive correlations, but the correlation coefficient (R^2) values differ. For example, the correlation coefficient (R^2) between the width and thickness for tongue-shaped debris deposits is 0.9731, whereas that for distributary channels is 0.6438 (Fig. 9B). To further understand controls on the scale of distributary channels, cross plots associated with locations of distributary channels (Fig. 10) and lithofacies in these channels were created (Fig. 11). As shown in Fig. 10, thicker single gravel-sand deposits, lighter color of mudstone and higher V/Ni ratio indicate shallower water (Jones & Manning, 1994), thus, the lake level rises first and then falls (SQ1–SQ4: relatively deep water; SQ5: medium water depth; SQ6: relatively shallow water). These plots

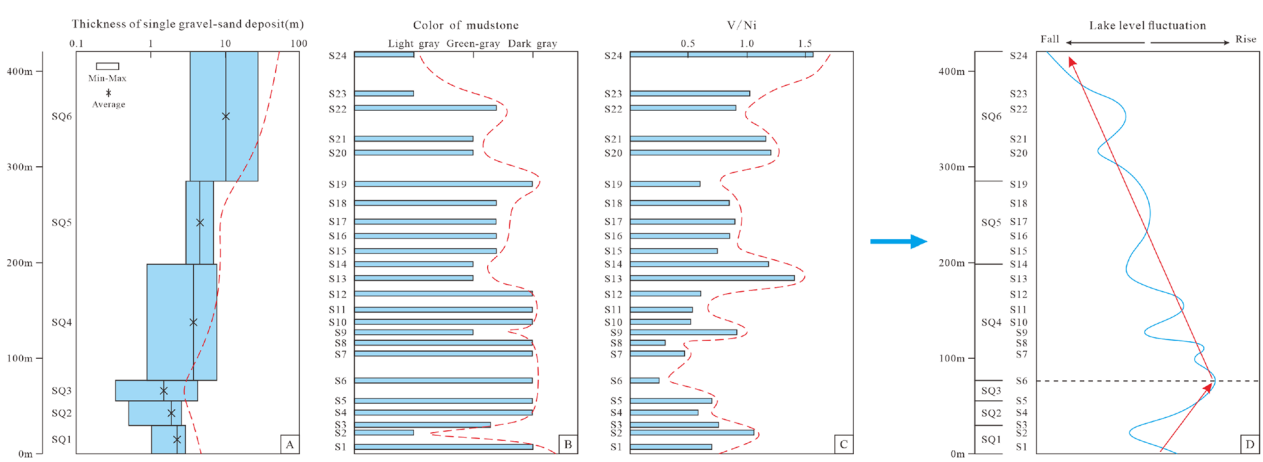

Fig. 10 Lake level fluctuation of studied section. **A** Thickness variations of single gravel-sand deposits. Thinner gravel-sand deposits indicate shallower water; **B** Mudstone color variations, a lighter color indicates shallower water; **C** Major and trace elements content variations, the V/Ni ratio is negatively correlated to the water depth, thus, a higher value indicates shallower water (Jones & Manning, 1994); and **D** The lake level fluctuation is inferred based on (**A**, **B** and **C**). SQ1–SQ4: relatively deep water; SQ5: medium water depth; SQ6: relatively shallow water

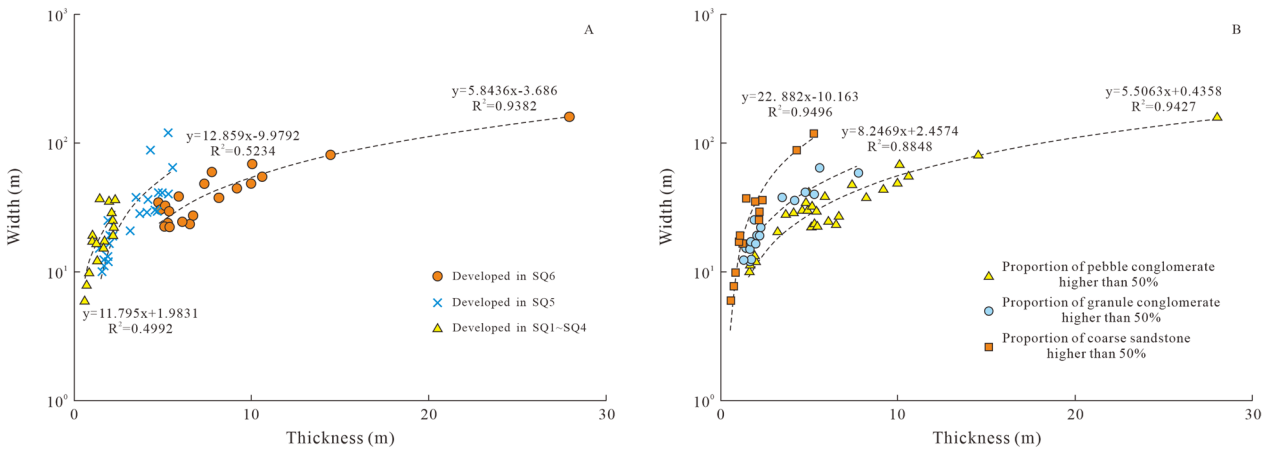

Fig. 11 Control of lake level fluctuation and lithofacies on dimensions of distributary channels. **A** The channels developed in shallower water are characterized by thicker layer and lower width/thickness ratio. **B** Coarser-grained distributary channels with larger thickness and lower width/thickness ratio

reveal the following: (i) Distributary channels that developed in shallower waters are characterized by thicker layers and lower width/thickness ratios, and these highlight the influence of lake level fluctuations on the channel-related erosion. These channels that developed in shallower waters are more incised because of a low resistance of water bodies and highly concentrated flows (Fig. 11A). (ii) Coarser-grained distributary channel deposits are thicker and these exhibit lower width/thickness ratios because of the intense erosion associated with coarse sediments (Fig. 11B).

5 Factors controlling the vertical grain-size trend of mouth bar

As stated in Sect. 4.2, the vertical grain-size trends of mouth bar accretions are complex. Gravel accretions commonly show fining-upward trends, whereas sand accretions exhibit coarsening-upward trends (Fig. 6). Grain size analyses of samples selected from mouth bar accretion involving diverse vertical variations reveal that grain sizes of sediments control vertical grain-size trends. Accretions involving coarse sediments (median grain size > 1000 μm) commonly display a fining-upward trend, whereas those containing fine sediments (median grain size < 1000 μm) exhibit a coarsening-upward trend in the Sangyuan section (Fig. 12).

The deposition of sediments in a river-mouth system is associated with the effluent behavior, which is affected by both the inertia and bed friction. An inertia-dominated effluent increases grain sizes of sediments along foreset beds, and thus, the associated mouth bar accretions are characterized by a fining-upward trend. Conversely, a friction-dominated effluent decreases grain sizes of sediments along foreset beds, and the corresponding accretions

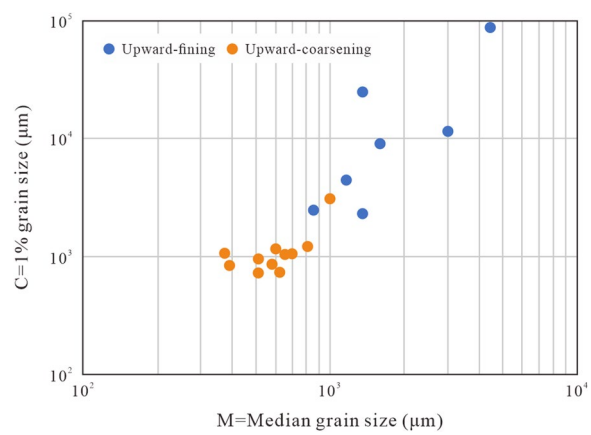

Fig. 12 Vertical grain-size trend of mouth bar accretions varies with grain size. Accretions involving coarse-grained sediments (median grain size is > 1000 μm) display fining-upward trends, whereas those with fine-grained sediments (< 1000 μm) are characterized by inverse grading

display a coarsening-upward trend (Postma, 1990; Wang et al., 2015; Wright, 1977). The relative strengths of the inertial force and bed friction in a river-mouth system are strongly connected to the Reynolds (*Re*) and Froude (*Fr*) numbers (Wright, 1977). An inertia-dominated depositional pattern occurs if the *Re* exceeds 2300 or if the *Fr* is > 16.1, whereas lower *Re* and *Fr* values are linked to friction-dominated processes (Barkley et al., 2015; Hayashi et al., 1967). The parameters *Re* and *Fr* can be calculated using the following expressions:

$$Re = \frac{vh}{\mu} \tag{1}$$

$$Fr = \frac{v}{\sqrt{gh}} \tag{2}$$

where v is the flow velocity (m sec $^{-1}$) that is related to the discharge, slope of the substrate layer, etc. A high discharge and a steep slope of the substrate layer cause a high flow velocity, thereby producing high *Re* and *Fr* values, as validated by Zhang et al. (2021) using flume experiments. The parameter μ is the kinematic viscosity (m^2 sec^{-1}), which is mainly affected by grain size of sediments. Fine sediments elevate the viscosity, thereby creating low *Re* values, as reported by Zhang et al. (2021). The parameter h is water depth of channel outlet (m) and g is the gravitational constant (m sec^{-2}). Therefore, gravel accretions in mouth bars that are characterized by normal grading can be considered as products of inertia-dominated effluents because of their high *Re* values. As the *Re* value decreases, sand accretions in river-mouth systems display a coarsening-upward trend, and this highlights the control of friction-dominated effluents.

As for the overall vertical grain-size trend of mouth bar, it depends on the stacking pattern of accretions rather than the grading sequence of one accretion. In the Sangyuan section, four grading patterns are evident, including an overall inverse grading that involves repetitive coarsening-upward packages (Fig. 13), an overall inverse grading comprising inversely- and normally-graded accretions (Fig. 6C), an overall inverse grading showing a repetition of fining-upward packages (Fig. 13), and an overall normal grading that comprises repeating fining-upward packages (Fig. 6B). The overall inverse grading of the mouth bar deposits is attributed to overlying coarser accretions, whereas the decline in sediment sizes in bottom-up accretions can produce overall normally graded mouth bar.

6 Conclusions

The main findings of this study are summarized as follows:

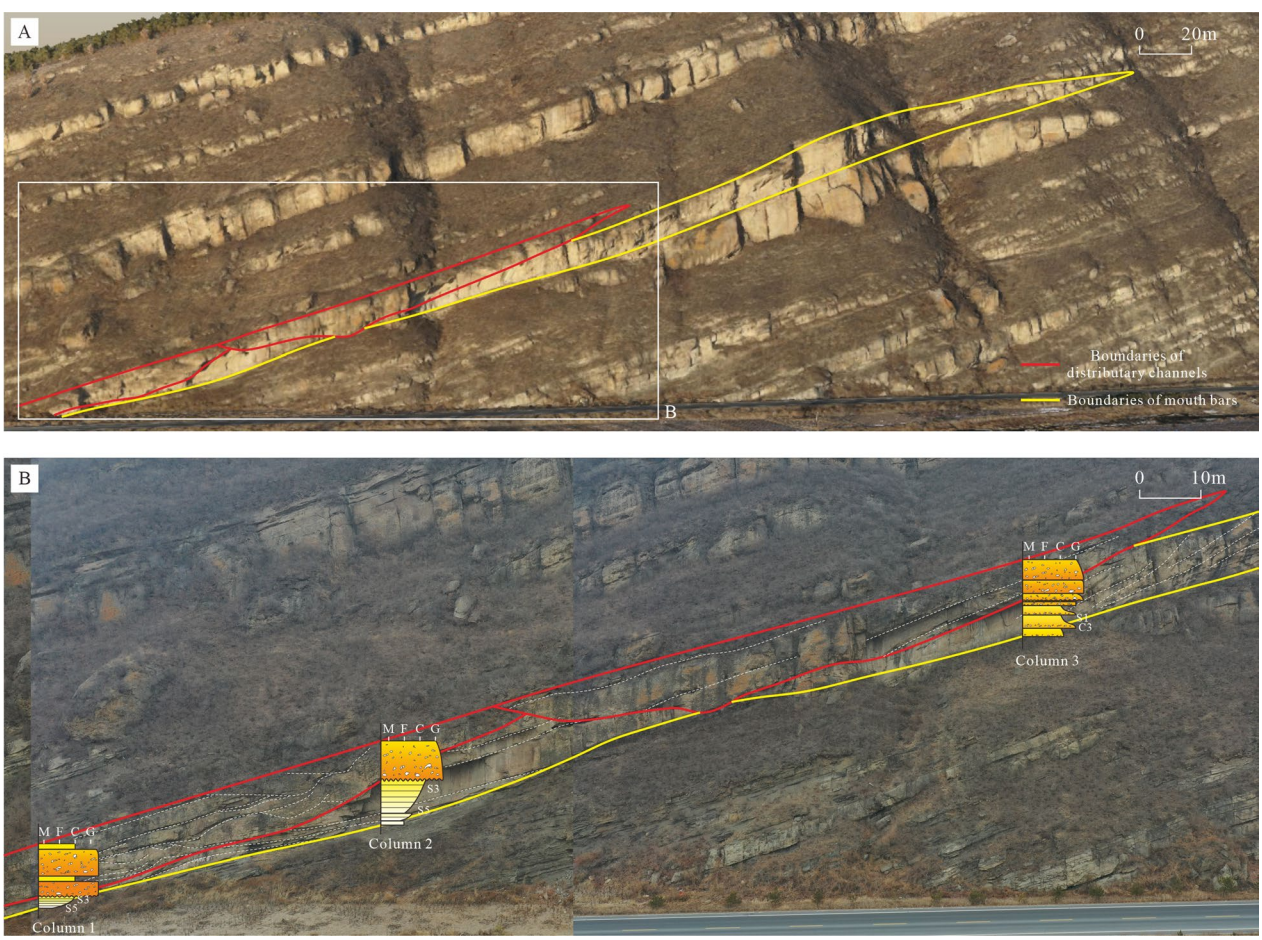

Fig. 13 Overall inverse grading of mouth bar. In Columns 1 and 2, the overall inverse grading is characterized by repeated coarsening-upward packages, whereas in Column 3, the inverse grading involves repeated fining-upward packages

(1) Five facies associations are interpreted in gravel-sand deposits in the Sangyuan section, including subaerial distributary channels, subaqueous distributary channels, tongue-shaped debris deposits, mouth bars and sheet sands. Mouth bar consists of gravel and sand accretions, showing coarsening-upward trend or fining-upward trend. Facies associations displayed differences in dimensions, which indicated variations in flow conditions during deposition. Overall, the width/thickness ratios of facies associations increased rapidly as the flow energy and flow concentration changed from those of debris flows to traction currents during evolution of the shallow-water fan delta. Variations in flow conditions during deposition of sediments in subaqueous distributary channels and mouth bars can explain the wide differences in width/thickness ratios.
(2) In the gravel-sand deposits of the Sangyuan section, both distributary channels and mouth bars dominate facies associations of the shallow-water fan-delta front, accounting for 53.42% and 36.88%, respectively. Tongue-shaped debris deposits and sheet sands represent 8.39% and 1.31%, respectively.
(3) Grain sizes of sediments influence the strength of the inertial force and bed friction during deposition, and these factors determined the behavior of effluents in the river-mouth system, which further result in the vertical grain-size trends of mouth bar accretions. The normal grading of gravel accretions was attributed to inertia-dominated effluents. Sand accretions displayed a coarsening-upward trend in the river-mouth system, and this was assigned to friction-dominated effluents. The overall vertical grain-size trend of mouth bars depended on the stacking pattern of accretions rather than the grading in one accretion. The overall inverse grading of the mouth bar deposits is attributed to overlying coarser accretions, whereas the decline in sediment sizes in bottom-up accretions accounted for overall normally graded mouth bar.

Acknowledgements
We thank our colleague Yunjie Xu for the helpful discussion and feedback.

Author contributions
KZ and SW contributed the central idea, analyzed most of the data, and wrote the initial draft of the paper. The remaining authors contributed to refining the ideas, carrying out additional analyses and finalizing this paper. All authors read and approved the final manuscript.

Funding
This project is supported by the National Natural Science Foundation of China (No. 42272110).

Availability of data and materials
All relevant raw data will be freely available to any scientist wishing to use them for non-commercial purposes, without breaching participant confidentiality.

Declarations

Ethics approval and consent to participate
Not applicable.

Consent for publication
Not applicable.

Competing interests
The authors declare that they have no competing interests.

Received: 17 October 2022 Accepted: 16 February 2023
Published online: 24 May 2023

References

Backert, N., Ford, M., & Malartre, F. (2010). Architecture and sedimentology of the Kerinitis Gilbert-type fan delta, Corinth Rift, Greece. *Sedimentology, 57*, 543–586.
Barkley, D., Song, B. F., Mukund, V., Lemoult, G., Avila, M., & Hof, B. (2015). The rise of fully turbulent flow. *Nature, 526*, 550–553.
Barrett, B. J., Collier, R. E. L., Hodgson, D. M., Gawthorpe, R. L., Dorrell, R. M., & Cullen, T. M. (2019). Quantifying faulting and base level controls on syn-rift sedimentation using stratigraphic architectures of coeval, adjacent Early-Middle Pleistocene fan deltas in Lake Corinth, Greece. *Basin Research, 31*(6), 1040–1065.
Benvenuti, M. (2003). Facies analysis and tectonic significance of lacustrine fan-deltaic successions in the Pliocenee–Pleistocene Mugello Basin, Central Italy. *Sedimentary Geology, 157*, 197–234.
Billi, P., Magi, M., & Sagri, M. (1991). Pleistocene lacustrine fan delta deposits of the Valdarno Basin Italy. *Journal of Sedimentary Petrology, 61*(2), 280–290.
Blair, T. C., & McPherson, J. G. (1998). Recent debris-flow processes and resultant form and facies of the dolomite alluvial fan, Owens Valley, California. *Journal of Sedimentary Research, 68*(5), 800–818.
Blistan, P., Kovanič, Ľ, Zelizňaková, V., & Palková, J. (2016). Using UAV photogrammetry to document rock outcrops. *Acta Montanistica Slovaca, 21*(2), 154–161.
Colella, A. (1988). Fault-controlled marine gilbert-type fan deltas. *Geology, 16*(11), 1031–1034.
Cope, T. D., & Graham, S. A. (2007). Upper crustal response to Mesozoic tectonism in western Liaoning, North China, and implications for lithospheric delamination. *Geological Society London Special Publications, 280*(1), 201–222.
Cope, T., Luo, P., Zhang, X. Y., Zhang, X. J., Song, J. M., Zhou, G., & Shultz, M. R. (2010). Structural controls on facies distribution in a small half-graben basin: Luanping basin, northeast China. *Basin Research, 22*(1), 33c44.
Davis, G. A., Zheng, Y. D., Wang, C., Darby, B. J., Zhang, C. H., & Gehrels, G. (2001). Mesozoic tectonic evolution of the Yanshan fold and thrust belt, with emphasis on Hebei and Liaoning provinces, northern China. *Memoir of the Geological Society of America, 194*, 171–197.
Dou, L. X., Hou, J. G., Song, S. H., Zhang, L., Liu, Y. M., Sun, S., Li, Y. Q., Wang, X. X., Ren, X. X., Tang, Y., Tian, H., & Yang, Y. H. (2020). Sedimentary characteristics of hyperpycnites in a shallow lacustrine environment: A case study from the Lower Cretaceous Xiguayuan Formation, Luanping Basin, Northeast China. *Geological Journal, 55*(5), 3344–3360.
Dunne, L. A., & Hempton, M. R. (1984). Deltaic sedimentation in the Lake Hazar pull-apart basin, south-eastern Turkey. *Sedimentology, 31*, 401–412.
Edmonds, D. A., Shaw, J. B., & Mohrig, D. (2011). Topset-dominated deltas: A new model for river delta stratigraphy. *Geology, 39*(12), 1175–1178.
Ethridge, F. G., & Wescott, W. A. (1984). Tectonic setting, recognition and hydrocarbon reservoir potential of fan-delta deposits. In E. H. Koster & R. J. Steel

(Eds.), *Sedimentology of gravels and conglomerates* (pp. 217–236). Calgary: Canadian Society of Petroleum Geologists.
Fabbricatore, D., Robustelli, G., & Muto, F. (2014). Facies analysis and depositional architecture of shelf-type deltas in the Crati Basin (Calabrian arc, south Italy). *Italian Journal of Geosciences, 133*(1), 131–148.
Falk, P. D., & Dorsey, R. J. (1998). Rapid development of gravelly high-density turbidity currents in marine Gilbert-type fan deltas, Loreto Basin, Baja California Sur, Mexico. *Sedimentology, 45*, 331–349.
Gani, M. R. (2004). From turbid to lucid: A straightforward approach to sediment gravity flows and their deposits. *The Sedimentary Record, 2*(3), 4–8.
Gloppen, T. G., & Steel, R. J. (1981). *The deposits, internal structure and geometry in six alluvial fan-fan delta bodies (Devonian-Norway) a study in the significance of bedding sequences in conglomerates* (Vol. 31, pp. 49–69). Tulsa: Special Publications.
Graham, S. A., Hendrix, M. S., Johnson, C. L., Badamgarav, D., Badrach, G., Amory, J., Porter, M., Barsbold, R., Webb, L. E., & Hacker, B. R. (2001). Sedimentary record and tectonic implications of Mesozoic rifting in southeast Mongolia. *Geological Society of America Bulletin, 113*(12), 1560–1579.
Hampton, M. (1975). Competence of fine-grained debris flows. *Journal of Sedimentary Petrology, 23*(2), 213–234.
Hayashi, J., Shuto, N., & Kawakami, K. (1967). Basic study on the diffusion of warm water jets discharged from power plants into bays. *Coastal Engineering in Japan, 10*(1), 129–142.
Holmes, A. (1965). *Principles of physical geology* (pp. 288–289). London: Thomas Nelson and Sons.
Jia, A. L., Mu, L. X., Chen, L., & Huang, S. Y. (2000). Approach for detailed study of reservoir outcrop. *Acta Petrolei Sinica, 21*(4), 105–108. (in Chinese with English abstract).
Jia, H. B., Ji, H. C., Wang, L. S., Gao, Y., & Wang, Z. K. (2018). Controls of a Triassic fan-delta system, Junggar basin. *NW China. Geological Journal, 53*(6), 3093–3109.
Jia, H. B., Ji, H. C., Yu, J. F., & Meng, X. C. (2020). Sediment supply control on the delivery of sediments to deep-lacustrine environment: A case study from Luanping Basin, northern China. *Geological Journal, 55*(5), 3679–3693.
Jones, B., & Manning, D. A. C. (1994). Comparison of geochemical indices used for the interpretation of palaeoredox conditions in ancient mudstones. *Chemical Geology, 111*, 111–129.
Kim, S. B. (1995). Alluvial fans and their natural distinction from rivers based on morphology, hydraulic processes, sedimentary processes, and facies assemblages—discussion. *Journal of Sedimentary Research, 65*, 706–708.
Li, P. X., Liu, Y. Q., & Tian, S. G. (2004). Advances in the study of the Jurassic-Cretaceous lithostratigraphy in the Luanping Basin, northern Hebei. *Geological Bulletin of China, 23*(8), 757–765. (in Chinese with English abstract).
Liu, B. B., Tan, C. P., Yu, X. H., Qu, J. H., Zhao, X. M., & Zhang, L. (2019). Sedimentary characteristics and controls of a retreating, coarse-grained fan-delta system in the Lower Triassic, Mahu Depression, northwestern China. *Geological Journal, 54*(3), 1141–1159.
Longhitano, S. G. (2008). Sedimentary facies and sequence stratigraphy of coarse-grained Gilbert-type deltas within the Pliocene thrust-top Potenza Basin (Southern Apennines, Italy). *Sedimentary Geology, 210*(3–4), 87–110.
Lowe, D. R. (1982). Sediment gravity flows, II: Depositional models with special reference to the deposits of high-density turbidity currents. *Journal of Sedimentary Petrology, 52*(1), 279–297.
Luo, P. (2007). *Proceedings of key laboratory of oil and gas reservoir in 2004–2005* (pp. 142–154). Beijing: Petroleum Industry Press.
McConnico, T. S., & Bassett, K. N. (2007). Gravelly Gilbert-type fan delta on the Conway Coast, New Zealand: Foreset depositional processes and clast imbrications. *Sedimentary Geology, 198*(3–4), 147–166.
McPherson, J. G., Shanmugam, G., & Moiola, R. J. (1987). Fan-deltas and braid deltas: Varieties of coarse-grained deltas. *Geological Society of America Bulletin, 99*(3), 331–340.
Nemec, W., & Steel, R. J. (Eds.). (1988). *Fan Deltas: Sedimentology and Tectonic Setting* (p. vii-ix (444)). London: Blackie and Son.
Orton, G. J., & Reading, H. G. (1993). Variability of deltaic processes in terms of sediment supply, with particular emphasis on grain size. *Sedimentology, 40*, 475–512.
Pöppelreiter, M., & Aigner, T. (2003). Unconventional patterns of reservoir facies distribution in epeiric successions: Lessons from an outcrop analog (Lower Keuper, Germany). *AAPG Bulletin, 87*(1), 39–70.
Postma, G. (1990). An analysis of the variation in delta architecture. *Terra Nova, 2*(2), 124–130.
Postma, G., & Roep, T. B. (1985). Resedimented Conglomerates in the bottomsets of Gilbert-type gravel deltas. *Journal of Sedimentary Research, 55*(6), 874–885.
Rasmussen, H. (2000). Nearshore and alluvial facies in the Sant Llorenç del Munt depositional system: Recognition and development. *Sedimentary Geology, 138*(1–4), 71–98.
Ren, J. Y., Tamaki, K., Li, S. T., & Zhang, J. X. (2002). Late Mesozoic and Cenozoic rifting and its dynamic setting in eastern China and adjacent areas. *Tectonophysics, 344*(3–4), 175–205.
Rohais, S., Eschard, R., & Guillocheau, F. (2008). Depositional model and stratigraphic architecture of rift climax Gilbert-type fan deltas (Gulf of Corinth, Greece). *Sedimentary Geology, 210*(3–4), 132–145.
Shanmugam, G. (2000). 50 years of the turbidite paradigm (1950s–1990s): Deep-water processes and facies models-a critical perspective. *Marine and Petroleum Geology, 17*(2), 285–342.
Shultz, A. W. (1984). Subaerial debris-flow deposition in the Upper Paleozoic Cutler Formation, western Colorado. *Journal of Sedimentary Petrology, 54*(3), 759–772.
Sohn, Y. K., Rhee, C. W., & Kim, B. C. (1999). Debris flow and hyperconcentrated flood-flow deposits in an alluvial fan, northwestern part of the Cretaceous Yongdong Basin, Central Korea. *Journal of Geology, 107*(1), 111–132.
Tian, S. G., Pang, Q. Q., Niu, S. W., Li, P. X., & Liu, Y. Q. (2004). Terrestrial Jurassic-Cretaceous boundary stratotype candidate in Luanping Basin, northern Hebei. *Geological Bulletin of China, 23*(12), 1170–1179. (in Chinese with English abstract).
Turner, B. R., & Tester, G. N. (2006). The Table Rocks Sandstone: A fluvial, friction-dominated lobate mouth bar sandbody in the Westphalian B Coal Measures. *NE England. Sedimentary Geology, 190*(1–4), 97–119.
Van Dijk, M., Postma, G., & Kleinhans, M. G. (2009). Autocyclic behaviour of fan deltas: An analogue experimental study. *Sedimentology, 56*, 1569–1589.
Wang, J. H., Jiang, Z. X., Zhang, Y. F., Gao, L. M., Wei, X. J., Zhang, W. Z., Liang, Y., & Zhang, H. Y. (2015). Flume tank study of surface morphology and stratigraphy of a fan delta. *Terra Nova, 27*, 42–53.
Wei, H. H., Meng, Q. R., Wu, G. L., & Li, L. (2012). Multiple controls on rift basin sedimentation in volcanic settings: Insights from the anatomy of a small Early Cretaceous basin in the Yanshan belt, northern North China. *Geological Society of America Bulletin, 124*(3–4), 380–399.
Winsemann, J., Hornung, J. J., Meinsen, J., Asprion, U., Polom, U., Brandes, C., Bußmann, M., & Weber, C. (2009). Anatomy of a subaqueous ice-contact fan and delta complex, Middle Pleistocene, North-west Germany. *Sedimentology, 56*, 1041–1076.
Wright, L. D. (1977). Sediment transport and deposition at river mouths: A synthesis. *Geological Society of America Bulletin, 88*, 857–868.
Wu, F. D., Chen, Y. J., Li, Y., & Jiao, Y. Q. (2000). Tectonic evolutions and their control on development of fan-deltaic depositional system in the Luanping Basin. *Geoscience, 14*(2), 179–184. (in Chinese with English abstract).
Wu, S. H., Feng, W. J., Yin, S. L., Yu, C., & Zhang, K. (2016). Research advances in alluvial fan depositional architecture. *Journal of Palaeogeography, 18*(4), 497–512. (in Chinese with English abstract).
Wu, W., Li, Q., Pei, J. X., Ning, S. Y., Tong, L. Q., Liu, W. Q., & Feng, Z. D. (2020). Seismic sedimentology, facies analyses, and high-quality reservoir predictions in fan deltas: A case study of the Triassic Baikouquan Formation on the western slope of the Mahu Sag in China's Junggar Basin. *Marine and Petroleum Geology, 120*, 104546.
Yan, D. Z., Xu, H. M., Xu, Z. H., Lei, Z. C., Tian, M., Cheng, L., Ma, Y. H., Wang, Z. L., & Ostadhassan, M. (2020). Sedimentary architecture of hyperpycnal flow deposits: Cretaceous Sangyuan outcrop, from the Luanping Basin, North East China. *Marine and Petroleum Geology, 121*, 104593.
Yin, S. L., Tan, Y. Y., Zhang, L., Feng, W., Liu, S. Y., & Jin, J. (2018). 3D outcrop geological modeling based on UAV oblique photography data: A case study of Pingtouxiang section in Lüliang City, Shanxi Province. *Journal of Palaeogeography (Chinese Edition), 20*(5), 909–924. (in Chinese with English abstract).
Zavala, C., & Pan, S. X. (2018). Hyperpycnal flows and hyperpycnites: Origin and distinctive characteristics. *Lithologic Reservoirs, 30*(1), 1–18. (in Chinese with English abstract).

Zavala, C., Ponec, J. J., Arcuri, M., Drittanti, D., Freije, H., & Asensio, M. (2006). Ancient lacustrine hyperpycnites: A depositional model from a case study in the rayoso formation (cretaceous) of west-central Argentina. *Journal of Sedimentary Research., 76*(1), 41–59.
Zhang, K., Wu, S. H., Feng, W. J., Xu, Z. H., Wang, J. J., Zhang, J. J., & Peng, Y. J. (2021). Experimental study of fan delta evolution: Autogenic cycles of fully confined channelized flow and small secondary channelized flows. *Sedimentary Geology, 426*, 106024.
Zhang, K., Wu, S. H., Xu, Y. J., Xiong, Q. C., Gao, Z. J., & Yu, J. T. (2022a). Sedimentary characteristics of mouth bar within lacustrine fan delta: Insights from the Lower Cretaceous Xiguayuan Formation of Sangyuan outcrop, Luanping Basin. *Journal of Palaeogeography (Chinese Edition), 24*(3), 415–432. (in Chinese with English abstract).
Zhang, T., Yang, Z. H., & Sun, C. C. (2022b). Stochastic simulation of fan deltas using parallel multi-stage generative adversarial networks. *Journal of Petroleum Science and Engineering, 208*, 109442.
Zhong, X. A., Escalona, A., Sverdrup, E., & Bukta, K. E. (2018). Impact of fault evolution in Gilbert-type fan deltas in the Evrostini area, south-central Gulf of Corinth, Greece. *Marine and Petroleum Geology, 95*, 82–99.
Ziegler, M. A. (2001). Late Permian to Holocene paleofacies evolution of the Arabian plate and its hydrocarbon occurrences. *GeoArabia, 6*(3), 445–504.

Publisher's Note

Springer Nature remains neutral with regard to jurisdictional claims in published maps and institutional affiliations.

Submit your manuscript to a SpringerOpen journal and benefit from:

- ► Convenient online submission
- ► Rigorous peer review
- ► Open access: articles freely available online
- ► High visibility within the field
- ► Retaining the copyright to your article

Submit your next manuscript at ► springeropen.com